TSC22D4 interacts with Akt1 in response metabolic and stress signals

Sevgican Demir[1,2,3], Gretchen Wolff[1,2,3], Annika Wieder[1,2,3], Adriano Maida[1,2,3], Marco Rahm[4], Martina Schnölzer[5], Dominic Helm[5], Stefanie Hauck[4], Julia Szendrödi[1,2,3], Stephan Herzig[1,2,3], Bilgen Ekim Üstünel[1,2,3 *]

[1] Institute for Diabetes and Cancer (IDC), Helmholtz Diabetes Center, Helmholtz Center, Munich, Neuherberg, Germany

[2] Joint Heidelberg-IDC Translational Diabetes Program, Inner Medicine 1, Heidelberg University Hospital, Heidelberg, Germany

[3] German Center for Diabetes Research (DZD), Neuherberg, Germany

[4] Research Unit Protein Science, Helmholtz Center Münich, Neuherberg, Germany.

[5] German Cancer Research Center (DKFZ), Genomics and Proteomics Core Facility, Heidelberg Germany

* Corresponding Author: Bilgen Ekim Üstünel

bilgen.ekimuestuenel@med.uni-heidelberg.de

Conflict of interest statement: The authors have declared that no conflict of interest exists

Key Words: TSC22D4, insulin signaling, Akt, phosphorylation

Financial Support

This work was supported by Deutsche Forschungsgemeinschaft (DFG) EK 108/1-1 grant to B.E.Ü and DFG CRC 1118 grant to S.H.

Abstract

Transforming Growth Factor β 1 Stimulated Clone 22 D4 (TSC22D4) is an intrinsically disordered protein that regulates cellular and physiological processes such as cell proliferation, cellular senescence as well as hepatic glucose and lipid metabolism. The molecular mechanism of TSC22D4 action in these cellular and metabolic functions, however, remains largely elusive. Here, we identified TSC22D4 as a novel protein kinase B/Akt1 interacting protein, a critical mediator of insulin/PI3K signaling pathway implicated in diverse set of diseases including type 2 diabetes, obesity and cancer. TSC22D4 interacts with Akt1 not constitutively but rather in a regulatory manner. While glucose and insulin stimulation of cells or refeeding of mice impair the hepatic TSC22D4-Akt1 interaction, inhibition of mitochondria and oxidative stress, promote it; indicating that extra- and intra-cellular cues play a key role in controlling TSC22D4-Akt1 interaction. Our results also demonstrate that together with its dimerization domain, i.e. the TSC box, TSC22D4 requires its intrinsically disordered region (D2 domain) to interact with Akt1. To understand regulation of TSC22D4 function further, we employed tandem mass spectrometry and identified 15 novel phosphorylation sites on TSC22D4. Similar to TSC22D4-Akt1 interaction, TSC22D4 phosphorylation also responds to environmental signals such as starvation, mitochondrial inhibition and oxidative stress. Interestingly, 6 out of the 15 novel phosphorylation sites lie within the TSC22D4 D2 domain, which is required for TSC22D4-Akt1 interaction. Characterization of the regulation and function of these novel phosphorylation sites, in the future, will shed light on our understanding of the role of TSC22D4-Akt1 interaction in both cell biological and physiological functions. Overall, our findings postulate a model whereby TSC22D4 acts as an environmental sensor and interacts with Akt1 to regulate cell proliferation, cellular senescence as well as maintain metabolic homeostasis.

49 **Introduction**

50 Insulin signaling pathway is an evolutionarily conserved mechanism that plays a key function in
51 regulation of cell growth, cell proliferation, development, longevity, as well as metabolic homeostasis.
52 When insulin binds to the insulin receptor (IR), IR gets activated and phosphorylates insulin receptor
53 substrate (IRS) to initiate a cascade of phosphorylation events leading to activation of the
54 insulin/phosphatidyl inositol 3-kinase (PI3K) signaling mediated by Protein Kinase B (PKB)/Akt [1].
55 Once phosphorylated by PI3K-dependent kinase 1 (PDK1) and mechanistic target of rapamycin
56 complex 2 (mTORC2) on T308 and S473 respectively, Akt kinase becomes catalytically active and
57 phosphorylates a wide range of targets including glycogen synthase kinase 3β (GSK3β), forkhead box
58 O1 (FoxO1), tuberous sclerosis complex 2 (TSC2) to promote cell survival, cell growth and cell
59 proliferation, as well as to regulate glucose and lipid metabolism [2]. In addition to the phosphorylation
60 events, protein-protein interactions play a key role in regulating Akt function [3]. PtdIns-3,4,5-P3 (PIP3),
61 c-jun N terminal kinase interacting protein 1 (JIP1), growth factor receptor-binding protein 10 (Grb10),
62 Tribbles homolog 3 (Trb3) represent only a few of the proteins that interact with Akt to regulate its
63 distinct functions [3-5].

64 Elevated insulin levels during overnutrition initiates negative feedback loops in insulin signaling
65 pathway, leading to the pathological condition known as insulin resistance, in which metabolic organs
66 fail to respond to circulating insulin levels. Overnutrition also induces a chronic low-grade
67 inflammation which activates c-jun N terminal kinase (JNK) and inhibits AMP-activated protein kinase
68 (AMPK), contributing to pathogenesis of insulin resistance. When necessary measures such as
69 promoting weight loss via healthy eating and physical exercise are not taken, insulin resistance may
70 progress further into type 2 diabetes, which is hardly reversible and leads to several complications in
71 peripheral organs in the long run [6].

72 Recently, we identified Transforming Growth Factor β1 (TGFβ1) Stimulated Clone 22 D4 (TSC22D4) as
73 a regulator of Akt signaling pathway in mouse models of type 2 diabetes [7]. TSC22D4 belongs to TSC22

74 protein family, which contains the evolutionarily conserved TSC box with a leucine zipper motif. TSC22
75 family consists of 4 proteins: TSC22D1, TSC22D2, TSC22D3 and TSC22D4 with alternatively spliced
76 isoforms and they can homo- and heterodimerize with each other via leucine zipper motif in TSC Box
77 to regulate cell biological functions such as cellular senescence, cell proliferation and apoptosis [8-13].

78 Despite discovered two decades ago, our current knowledge on the regulation and function of
79 TSC22D4 remains very limited. TSC22D4 expression increases in cultured kidney cells upon osmotic
80 stress and TSC22D4 subcellular localization in neurons alters during stages of the embryonic
81 development and differentiation [10, 13]. TSC22D4 also suppresses cellular senescence by impairing
82 junB function [14]. Previously, we have shown that hepatic TSC22D4 expression increases upon liver
83 damage and cancer cachexia, and reprograms liver lipid metabolism [15]. Targeting TSC22D4
84 expression in the livers of mice with type 2 diabetes improves insulin-induced Akt phosphorylation,
85 alleviates insulin resistance and hyperglycemia [7]. Strikingly, in obese human patients, elevated
86 TSC22D4 expression in the liver positively correlates with insulin resistance [7]. These studies clearly
87 establish a novel and reciprocal connection between TSC22D4 and metabolic regulation, yet the
88 molecular mechanisms of this connection remains largely elusive.

89 Here, we identify TSC22D4 as a novel Akt1 interacting protein. Glucose stimulation of the starved cells
90 destabilizes the TSC22D4-Akt1 interaction, which is exacerbated further upon insulin stimulation.
91 Mitochondrial inhibition and oxidative stress, on the other hand, promote the TSC22D4-Akt1
92 interaction. To understand TSC22D4 regulation further, we employed liquid chromatography tandem
93 mass spectrometry (LC-MS/MS) and identified 15 novel phosphorylation sites on TSC22D4. Similar to
94 TSC22D4-Akt1 interaction, TSC22D4 phosphorylation also responds to both metabolic and stress
95 signals suggesting that TSC22D4 may act as a hub where it receives signals from different upstream
96 kinases to control intracellular crosstalk events. Overall, based on our findings, we propose a model in
97 which TSC22D4 acts as a signaling molecule that senses the environmental cues to interact with and
98 regulate Akt1 function.

99 **Results:**

100 **TSC22D4 interacts with Akt1**

101 In our previous studies, we showed that acute TSC22D4 knockdown promotes insulin induced Akt
102 phosphorylation both in cultured primary hepatocytes and in mouse livers. Interestingly, TSC22D4
103 knockdown also improves glucose handling and insulin sensitivity in diabetic mouse models [7]. To
104 study the function of TSC22D4 further, we generated hepatocyte specific TSC22D4 knockout mice
105 (TSC22D4$^{hep-/-}$) (Supp Fig. 1A). Similar to our previous findings, TSC22D4$^{hep-/-}$ mice had improved glucose
106 handling in glucose tolerance test and lower fasting blood glucose levels compared to TSC22D4$^{flox/flox}$
107 control mice when challenged with high fat diet without any changes in body weight (Supp Fig. 1B-D).
108 In primary hepatocytes isolated from TSC22D4$^{hep-/-}$ and TSC22D4$^{flox/flox}$ control mice, we observed that
109 TSC22D4 knockout cells had a much higher insulin induced phosphorylation of Akt and its direct
110 downstream targets GSK3β and FoxO1 as well phosphorylation of its indirect target S6K1, which agree
111 with our previous studies performed with shRNA-mediated TSC22D4 knockdown in primary
112 hepatocytes and livers (Supp Fig. 1E) [7].

113 To understand the molecular mechanisms of TSC22D4 action on insulin/Akt signaling pathway, we
114 examined the functional domains on TSC22D4 protein in detail. Interestingly, TSC22D4 does not have
115 any domains with known function other than its TSC box that contains a leucine zipper motif (Fig. 1A).
116 TSC box is common to all TSC22 family members and plays role in homodimerization or hetero-
117 dimerization of TSC22 family members with each other [8, 16]. By performing Clustal-omega analysis,
118 we identified two other regions (Region 1 and Region 2: R1 and R2) at TSC22D4 N-terminus which are
119 highly conserved from fish to mammals (Fig. 1A and Supp. Fig. 2) [17]. The primary sequence flanked
120 by R2 and TSC Box (105-308 aa) is also highly conserved between humans and mice, yet does not
121 contain any particular three-dimensional structure such as alpha-helices or beta sheets, hence fall into
122 the category of instrinsically disordered region (Fig. 1A and Supp. Fig. 2). Until recently, intrinsically
123 disordered regions were mainly ignored due to lack of a defined three-dimensional structure, yet these

124 regions contain many different post-translational modification (PTM) sites [18]. This diversity and
125 multiplicity of PTMs within intrinsically disordered regions allow proteins to acts as critical sensors of
126 the environmental cues as well as enable them to act as hubs for crosstlaking between signaling
127 pathways.

128 Since TSC22D4 contains a relatively long stretch of an intrinsically disordered region, we asked whether
129 TSC22D4 interacts with Akt to regulate its function. We prepared whole liver lysates from wild type
130 mice and immunoprecipitated endogenous TSC22D4. In western blots, we showed that endogenous
131 Akt1 was indeed enriched in endogenous TSC22D4 co-immunoprecipitates compared to IgG controls,
132 demonstrating that hepatic TSC22D4 and Akt1 interact *in vivo* in mouse livers (Fig. 1B). Unlike Akt1,
133 Akt2 levels in the TSC22D4 co-immunoprecipitates failed to enrich over IgG controls, suggesting that
134 TSC22D4 specifically interacts with Akt1 rather than Akt2 (data not shown).

135 In order to study the regulation of TSC22D4-Akt1 interaction more in detail, we employed
136 Hepa 1-6 cells. We transiently transfected Hepa 1-6 cells with Flag-TSC22D4 and HA-Akt1 plasmids and
137 repeated the co-IP experiments. As shown in Fig. 1C, HA-Akt1 co-IPed with Flag-TSC22D4 and
138 interestingly glucose stimulation impaired the TSC22D4-Akt1 interaction. Increasing glucose
139 concentration from 20 mM to 100 mM did not impair the TSC22D4-Akt1 interaction any further, but
140 additional stimulation of cells with 100 nM of insulin did (Fig. 1C, compare lanes 5-8 to 11-14). Very
141 interestingly, in the absence of glucose, insulin alone failed to disrupt the TSC22D4-Akt1 interaction
142 (Fig. 1C, compare lanes 9-10 to 11-14). Similar to glucose and insulin stimulation in the cells, refeeding
143 of wild type mice after an overnight starvation or i.p. insulin injection impaired the hepatic
144 TSC22D4-Akt1 interaction (Fig. 1D, 1E). Overall these data indicate that TSC22D4 is a novel Akt1
145 interacting protein and metabolic signals such as glucose and insulin stimulation impair the
146 TSC22D4-Akt1 interaction.

147 **Stress signals promote TSC22D4-Akt1 interaction**

148 Both in mice and in the cells, the TSC22D4-Akt1 interaction was strongest during starvation and was
149 impaired upon glucose and insulin stimulation. Since glucose availability promotes ATP generation, we
150 tested whether mitochondrial function regulates the TSC22D4-Akt1 interaction as well. We performed
151 Flag-TSC22D4 and HA-Akt1 co-IPs upon pharmacological inhibition of mitochondria with complex I
152 and III inhibitors, rotenone and antimycin, respectively. As shown in Fig. 2A, rotenone and antimycin
153 co-treatment (lanes 6-7) promoted the TSC22D4-Akt1 interaction and reduced
154 Akt-S473 phosphorylation while increasing AMPK-T172 phosphorylation confirming the increase in
155 AMP/ATP ratio upon drug treatments. Next, we asked whether inhibition of mitochondria promotes
156 TSC22D4-Akt1 interaction via AMPK activity. To this end, we employed U2OS-WT and
157 U2OS-AMPKα1/α2 double knockout (DKO) cells to transiently transfect Flag-TSC22D4 and HA-Akt1
158 plasmids and repeated co-IP experiments in the presence or absence of rotenone/antimycin. As shown
159 in Fig. 2B, lack of AMPK did not affect rotenone/antimycin induced TSC22D4-Akt interaction.
160 Additionally, glucose and insulin stimulation impaired TSC22D4-Akt interaction to similar degree in the
161 presence or absence of AMPK (Fig. 2C). Overall these data suggest that glucose stimulation or inhibition
162 of mitochondria regulate TSC22D4-Akt1 interaction independent of AMPK signaling.

163 Mitochondrial dysfunction contributes to generation of reactive oxygen species and induces oxidative
164 stress. Hence, we asked whether treatment of cells with ROS would also have an effect on TSC22D4-
165 Akt1 interaction and indeed found out that H_2O_2 treatment of Hepa 1-6 cells robustly promoted
166 TSC22D4-Akt1 interaction (Fig. 2D). H_2O_2 treatment also induced JNK phosphorylation indicating the
167 activation of stress signals. Therefore, we also tested whether JNK directly regulates TSC22D4-Akt1
168 interaction. Interestingly, TSC22D4-Akt1 interaction remained completely intact in JNK1/2 DKO mouse
169 embryonic fibroblasts (MEF) demonstrating that TSC22D4-Akt1 interaction takes place independent of
170 JNK1/2 (data not shown). Overall, these data show that while anabolic signals such as glucose and
171 insulin stimulation impair the TSC22D4-Akt1 interaction, catabolic and stress signals promote it,
172 independent of AMPK and JNK signaling pathways, respectively.

173 **TSC22D4-Akt interaction requires TSC22D4 intrinsically disordered region**

174 To map the TSC22D4 domain(s) required for TSC22D4-Akt interaction, we created TSC22D4 deletion
175 mutants as depicted in Fig. 3A. Since the intrinsically disordered region region contains a relatively long
176 stretch of aminoacids, we arbitrarily splitted it into two as Domain 1 (D1) and Domain 2 (D2) (Fig. 3A).
177 We transiently co-transfected Hepa 1-6 cells with different Flag-TSC22D4 deletion mutants and HA-
178 Akt1. Deletion of R1 (ΔR1) and R2 (ΔR2) individually or together (ΔN) as well as deletion of the first half
179 of intrinsically disordered region i.e. ΔD1, did not impair TSC22D4's ability to interact with HA-Akt1
180 although ΔR2- and ΔN-TSC22D4 also expressed at very low levels compared to other TSC22D4 alleles
181 (Supp. Fig. 3A).

182 Unlike R1, R2 and D1 regions, deletion of D2 (ΔD2) or TSC box (ΔTSC), however, completely attenuated
183 the TSC22D4-Akt interaction (Fig. 3B). Even when the cells were treated with rotenone and antimycin
184 that boost the TSC22D4-Akt1 interaction, the ΔD2-TSC22D4 mutant failed to interact with Akt
185 completely (Supp. Fig. 3B). The D2 domain lies within the intrinsically disordered region and potentially
186 carries the necessary features of undergoing versatile PTM events to interact with different partner
187 proteins similar to other intrinsically disordered region proteins. The TSC box, however, plays a key
188 role in homodimerization which might also be critical for the TSC22D4-Akt1 interaction. Indeed the
189 Flag-TSC22D4-ΔTSC mutant failed to dimerize with full length myc-TSC22D4, confirming the
190 requirement of TSC box for TSC22D4 homodimerization (Supp. Fig. 3C). The ΔD2-TSC22D4, on the other
191 hand, still managed to homodimerize with myc-TSC22D4, albeit to a less extent compared to wild type
192 Flag-TSC22D4 (Supp. Fig. 3D). Overall, these data suggest that TSC domain might have an indirect role
193 in mediating TSC22D4-Akt1 interaction via homodimerization.

194 Next, we generated the D2+TSC mutant to address whether it will be sufficient to interact with Akt1.
195 Indeed the D2+TSC allele interacted with Akt1 at stronger levels compared to WT-TSC22D4 (Fig. 3A,
196 Fig. 3C, Supp Fig. 3E).Next, we created the D2 domain and TSC box alone truncated mutants and
197 repeated the co-IP experiments. Interestingly, while D2 domain alone succesfully interacted with Akt1,
198 the TSC box alone failed to do so (Fig. 3D). Overall, these data show that although both D2 domain
199 and TSC box are required to interact with Akt, only D2 domain is sufficient to maintain the interaction.

200 **TSC22D4 undergoes phosphorylation**

201 During experiments in which we inhibitied mitochondria with rotenone and antimycin, we observed
202 that the Flag-TSC22D4 signal collapsed to a one single band at a lower molecular weight in the western
203 blots, indicating the loss of certain PTMs (Fig. 2A, 2B). Similar to the overexpressed Flag-TSC22D4,
204 endogenous TSC22D4 also behaved in a similar manner, and lost PTMs upon overnight starvation both
205 in Hepa 1-6 and AML12 cells (Fig. 4A and B). As opposed to rotenone and antimycin, H_2O_2 treatment
206 caused a massive shift in TSC22D4 signal to a higher molecular weight, indicating the introduction of
207 new PTM events (Fig. 2D). Previous studies also predicted that TSC22D4 might contain several
208 phosphorylation sites by in silico analysis [9]. To address, whether it is the phosphorylation events that
209 cause the shifts in TSC22D4 western blots, we performed an *in vitro* λ phosphatase assay on
210 immunoprecipitated Flag-TSC22D4. Upon λ phosphatase treatment, the Flag-TSC22D4 signal indeed
211 shifted to a lower molecular weight, confirming that TSC22D4 undergoes phosphorylation (Fig. 4C,
212 compare lanes 4-5 and 10-11).

213 Interestingly, although oxidative stress and mitochondrial inhibition caused opposite effects on
214 TSC22D4 phosphorylation, they both promoted the TSC22D4-Akt1 interaction, indicating that the
215 general hyper- or hypo-phosphorylation status of TSC22D4 does not necessarily direct the TSC22D4-
216 Akt1 interaction. Instead, these phosphorylation events might act in a specific manner depending on
217 the direct upstream regulators and control TSC22D4 function accordingly. Hence, we decided to
218 identify the exact amino acid residues on TSC22D4 that undergo phosphorylation. By employing liquid
219 chromatography tandem mass spectrometry (LC-MS/MS) we identified 15 novel phosphorylation sites
220 on TSC22D4 either in Hepa 1-6 cells or in in mouse livers which were highly conserved (Supp. Fig. 2 and
221 Fig. 4D). Interestingly, 6 out of 15 phosphorylation sites lie within the TSC22D4 D2 domain which is
222 required and sufficient to maintain TSC22D4-Akt1 interaction (Fig. 4D). Hence in the future it will be
223 extremely critical to address: **a.** Whether these phosphorylation sites also play role in TSC22D4-Akt1
224 interaction and **b.** If yes, to identify the responsible kinases. Addressing these questions will certainly
225 help us unravel the functional significance of TSC22D4-Akt1 interaction in regulating Akt1 function.

226 **Discussion**

227 Type 2 diabetes is a chronic and progressive disorder characterized by elevated blood glucose levels.
228 Although a wide range of type 2 diabetes medications exits, they all have their limitations and side
229 effects. Hence, a better understanding of molecular mechanisms that govern the pathogenesis of
230 insulin resistance and type 2 diabetes, will help development of more effective therapies. Recently, we
231 identified that TSC22D4 impairs insulin-induced Akt phosphorylation and exacerbates diabetic
232 hyperglycemia and insulin resistance [7]. The exact molecular mechanisms of TSC22D4 action in
233 metabolic control however remained poorly defined. Here, we discovered that TSC22D4 is a novel Akt1
234 interacting protein and TSC22D4-Akt1 interaction responds to metabolic signals such glucose and
235 insulin. Intriguingly, TSC22D4 interacts specifically with Akt1, but not with Akt2 (data not shown),
236 which may explain isoform specific functions that are governed only by Akt1 but not by Akt2 or vice
237 versa. Our data also pointed out to an interesting interplay between glucose and insulin stimulations
238 in controlling TSC22D4-Akt1 interaction. Insulin weakened the TSC22D4-Akt1 interaction only in the
239 presence of glucose and was not sufficient to modulate TSC22D4-Akt1 interaction on its own (Fig. 1C).
240 This single observation leads to at least two intriguing conclusions:

241 1. Glucose availability renders the TSC22D4-Akt1 interaction insulin-sensitive via yet-to-be
242 identified mechanisms.
243 2. Akt S473 phosphorylation does not (or is not sufficient to) blunt TSC22D4-Akt1 interaction in
244 the absence of glucose.

245 Unlike in glucose starved cells, insulin injection to the fasted mice did abolish the TSC22D4-Akt1
246 interaction, indicating that even low amounts of blood glucose levels during fasting is sufficient to
247 prime the insulin-induced dissociation of TSC22D4-Akt1 interaction (Fig. 1E). Together with our
248 previous data showing that hepatic TSC22D4 regulates hyperglycemia and insulin sensitivity, we are
249 tempted to hypothesize that TSC22D4 controls glucose metabolism via its interaction with Akt1.

250 TSC22D4 contains a long stretch of intrinsically disordered region. Recent evidence indicates that
251 proteins with intrinsically disordered regions act as critical environmental sensors [19]. Particularly,
252 multiple posttranslational modifications in the intrinsically disordered regions enable protein-protein
253 interactions and promote crosstalk between different signaling pathways Our observations indeed
254 support the notion that TSC22D4 might also acts as an environmental sensor because TSC22D4-Akt1
255 interaction and TSC22D4 phosphorylation also respond to intra- or extra-cellular cues. Interestingly
256 while both mitochondrial inhibition and oxidative stress promoted the TSC22D4-Akt1 interaction, each
257 had opposite effects on TSC22D4 phosphorylation, indicating that these phosphorylation events act in
258 a rather specific manner to regulate the TSC22D4-Akt1 interaction. In other words, the general hypo-
259 or hyper-phosphorylation status of TSC22D4 does not necessarily control the degree of TSC22D4-Akt1
260 interaction. Interestingly 6 out of the 15 novel phosphorylation sites that we identified on TSC22D4 lie
261 within the D2 domain, which is both required and sufficient to maintain the TSC22D4-Akt1 interaction.
262 Hence, it will be very intriguing to identify, in the future, whether these phosphorylations play a direct
263 role in maintaining TSC22D4-Akt1 interaction and if so, it will be critical to generate the phospho-
264 specific antibodies and identify the responsible kinases and signaling pathways.

265 TSC22D4 also needs its TSC box to interact with Akt1 (Fig. 3B). TSC box contains a leucine zipper motif
266 which enables its homodimerization or potentially its heterodimerization with other TSC22 family
267 members. Hence, rather than the TSC box per se, TSC22D4 might actually require to homodimerize or
268 heterodimerize to interact with Akt1. Indeed, in the *in vitro* binding assays we performed with purified
269 recombinant TSC22D4 and Akt1 proteins, TSC22D4 and Akt1 did not interact with each other (data not
270 shown), suggesting that TSC22D4 does not interact with Akt1 directly but rather involves other
271 proteins. Considering the fact that other TSC22 family members and Akt share many common
272 functions, it will be interesting, in the future, also to address the possibility of protein-protein
273 interactions between other TSC22 family members and Akt isoforms.

274 Based on our findings in this study, we postulate a working model, whereby TSC22D4 acts as a sensor
275 of metabolic and stress signals to interact with Akt1 and regulate its function. Nevertheless, current
276 evidence we present in this study is not adequate to conclude whether the TSC22D4-Akt1 interaction
277 is beneficial or harmful for metabolic health. It might as well have a dual function in a condition-
278 dependent manner. It will be interesting to unravel, in the future, the direct implications of TSC22D4-
279 Akt1 interaction in pathogenesis of several diseases such as metabolic syndrome that involve insulin
280 resistance and type 2 diabetes as well as carcinogenesis, in which dysregulated Akt function plays a
281 key role.

282 **Materials and Methods**

283 **1. Animal experiments**

284 Male albumin-cre mice crossed to the TSC22D4 floxed/floxed line (C57Bl/6N background) [20] were
285 housed at room temperature with 12h light-dark cycle on control diet (Research diets, New Brunswick,
286 NJ, USA, D12450B), 60% high fat diet (Research diets, D12492i) with Sucrose Containing Drinking Water
287 (42 g/l) or chow diet (10% energy from fat, Research Diets D12450Ji, USA) for weeks indicated for each
288 study. Mice had *ad libitum* access to food and water and were weighed regularly and inspected daily
289 for general health. All experiments were performed in accordance with the European Union directives
290 and the German animal welfare act (Tierschutzgesetz) and were approved by local authorities
291 (Regierungspräsidium Karlsruhe, license #G117/18 or #G116/18).

292 For adenovirus injections, 2×10^{9} plaque-forming units (p.f.u.) per recombinant virus were administered
293 via tail vein injection. In each experiment, 4-12 animals received identical treatments and were
294 analyzed under fasted, random fed or fed conditions as indicated. Organs including liver, epididymal
295 and inguinal fat pads, and gastrocnemius muscles were collected after specific time periods, weighed,
296 snap-frozen and used for further analysis.

297 AAVs were injected via tail vein at a dose of at $1x10^{1o}$ vector genome/mouse. Before sacrificing post
298 12-week of AAV injection, mice were starved for 6 h and followed by i.p. injection with 1.5U insulin per

299 kg body weight for 10 min. Organs including liver, epididymal fat pads, kidney, pancreas and
300 gastrocnemius muscles were collected after specific time periods, weighed, snap frozen and used for
301 further analysis. In each animal experiment, mice were randomly assigned to each group.

302 During animal group allocation animals in each group had similar mean and median body weight as
303 well as fasting blood glucose levels.

304 **2. Recombinant viruses**

305 Adenoviruses expressing the Flag-TSC22D4 cDNA under the control of the CMV promoter was cloned
306 using the BLOCK-iT Adenoviral expression system (Invitrogen). Viruses were purified by the cesium
307 chloride method and dialysed against phosphate-buffered-saline buffer containing 10% glycerol
308 before animal injection, as described [21].

309 For generating AAVs with cDNAs of TSC22D4 alleles (WT or ΔD2) were amplified with the following
310 primer pairs followed by Nhe1 and Xba1 digestion and subcloning into pdsAAV-LP1 plasmid:
311 TSC22D4-AAV-F with NheI: gatgctagcgtgtgctggaattctg, TSC22D4-AAV-R with XbaI:
312 gcatctagactcgagtcagatggaggg. The successful clones sequenced for confirmation with the following
313 primers: pdsAAV-TSC-F: ctgataggcacctattggtc, pdsAAV-TSC-R: ccacaactagaatgcagtg. Once the
314 sequence is confirmed, the plasmids were purified by using Qiagen Megaprep kit (#12381) according
315 to the manufacturer's instructions and sent to Vigene Biosciences (Maryland, USA) for AAV generation,
316 purification, and titration.

317 **3. Primary hepatocyte isolation and treatment**

318 Primary hepatocytes were isolated as previously described [22, 23]. To investigate insulin signaling
319 pathway, primary hepatocytes were seeded to collagen coated 6-well plates ($1x10^6$ cells per well) in
320 William´s medium (Pan Biotec, #P04-29510) supplemented with 2 mM L-Glutamine,
321 100 nM Dexamethasone, 10% Fetal Bovine Serum (FBS, life technologies, #10270-106) and 1%
322 penicillin-streptomycin (PenStrep, Life Technologies, #15140122). After 4 hours, the cells were washed

323 2 times with phosphate buffered saline (PBS) to get rid of the cells which do not attach to the surface.
324 After 48 hours, the cells were collected in 180 *µl of* 1.5x sample buffer, boiled at 95° for 5 minutes and
325 kept at -20°C until use for western blotting.

326 **4. Cell lines and cell culture**

327 Alpha mouse liver 12 (AML12, ATCC, CRL-2254), U2 osteosarcoma (U2OS, ATCC, HTB-96), Hepatoma
328 1-6 (Hepa1-6) (ATCC, CRL-1830) and human embryonic kidney 293A (HEK293A) cell lines were used.
329 AML12 cells were maintained in DMEM:F12 (ATCC, #302006) medium supplemented with 10% Fetal
330 Bovine Serum (FBS, life technologies, #10270-106), insulin-transferrin-selenium mix (ITS mix, Gibco,
331 #41400045) and 40 ng/ml dexamethasone (Sigma, #D8893). U2OS (wild type and AMPK α1/α2 double
332 knock out) cells were a kind gift from Reuben Shaw (Salk Institute for Biological Studies, San Diego, CA,
333 USA) and were maintained in DMEM supplemented with 10% FBS. Hepa1-6 and HEK293A cells were
334 maintained in Dulbecco's modified Eagle's medium (DMEM, Gibco, #11995) supplemented with
335 10% heat inactivated FBS and 50 U/ml penicillin-streptomycin (PenStrep, Life Technologies,
336 #15140122). HEK293A cells (Thermo Fischer Scientific, #R70507) cells were used to generate
337 adenoviruses. All the cell lines were maintained at humidified 37°C incubator containing 5% CO_2.

338 **5. Plasmid DNA transfection**

339 pcDNA3-HA-Akt1 plasmid was a kind gift from Dr. Diane Fingar (University of Michigan, Ann Arbor,
340 USA). Expression vectors of wild type (WT)-TSC22D4 and deletion mutants of TSC22D4 were created
341 using pcDNA3 plasmid backbone. For deletion mutants, site directed mutagenesis experiments were
342 performed with standard PCR-based methods (NEB, #E0554S) using corresponding primer sets:

Deletion Mutants	**Forward Primer**	**Reverse Primer**
TSC22D4-ΔR1	GAGGGCCCAGGAAGCCCAG	GGCCGCTGGCTTGTCATCGTC
TSC22D4-ΔR2	GAGCCTCCAAGCTTCGGT	GGCAGGGGCTCCAGGT
TSC22D4-ΔN	GAGCCTCCAAGCTTCGGT	GGCCGCTGGCTTGTCATCGTC

TSC22D4-ΔD1	ACCCTGCCCTCTCTGAGG	GCTTGGAGGCTCCAGATC
TSC22D4-ΔD2	GACTTGGTGAAGTCCCAC	CTGAGCACTATCTCCAGT
Truncation Mutants		
D2+TSC	GGAGATAGTGCTCAGACCCTG	GGCCGCTGGCTTGTCATCGTC
D2 domain	CCCTCTGCACCCAATGGGC	CATGGCTTGTTCAATCTTGTTGT
TSC Box	GACTTGGTGAAGTCCCACCTCATG	GGCCGCTGGCTTGTCATCGTC

343 Plasmids expressing TSC22D4 alleles and Akt1 were transiently co-transfected to Hepa1-6 cells using
344 Lipofectamine 2000 (Invitrogen, #11668019) according to the manufacturer's instructions. For
345 starvation experiments: 30-hour post transfection, the cells were starved in no glucose containing
346 RPMI medium in the absence of FBS (Gibco, #11879020) overnight and the next day cells were pre-
347 stimulated with glucose [20 mM] for 30 minutes and with insulin [100 nM] for an additional 30 minutes
348 followed by cell lysis. For experiments that did not involve starvation, cells were lysed 48-hour post
349 transfection. For U2OS cells, the same transfection protocol was followed except that the cells were
350 starved for 6 hours.

351 **6. Identification of TSC22D4 Phosphorylation Sites**

352 a. In cultured cells:

353 *Tryptic digestion and phosphopeptide enrichment*

354 Total cell lysates equivalent to 300 µg of protein per condition were used for a chloroform-methanol
355 precipitation for sample clean up. Followed by a standard in-solution digestion using Trypsin in
356 a 1:100 ratio. The resulting peptides were enriched for phosphorylation using TiO_2 beads. Prior to MS
357 analysis, the peptides were resuspended in 0.1% TFA/0.25% hexafluoroisopropanol.

358 *Mass spectrometry*

359 Tryptic peptides mixtures were separated using a nano Acquity UPLC system (Waters GmbH, Eschborn,
360 Germany). Peptides were trapped on a nano Acquity C18 column (180 µm x 20 mm, particle size 5 µm)
361 (Waters GmbH, Eschborn, Germany). The liquid chromatography separation was performed on a C18

362 column (BEH 130 C18 100 µm x 100 mm, particle size 1.7 µm (Waters GmbH, Eschborn, Germany))
363 with a flow rate of 400 nL /min. For all gel slices samples, the chromatography was carried out using a
364 3h gradient of solvent A (98.9% water, 1% acetonitrile, 0.1 % formic acid) and solvent B (99.9%
365 acetonitrile and 0.1% formic acid) in the following sequence: from 0 to 4% B in 1 min, from 4 to 30% B
366 in 140 min, from 30 to 45% B in 15 min, from 45 to 90% B in 5 min, 10 min at 90% B, from 90 to 0% B
367 in 0.1 min, and 9.9 min at 0% B. The nanoUPLC system was coupled online to an LTQ Orbitrap XL mass
368 spectrometer (Thermo Scientific, Bremen, Germany). The mass spectrometer was operated in the
369 sensitive mode with the following parameters: capillary voltage 2400V; capillary temperature 200°C,
370 normalized collision energy 35 V, activation time 30000 ms. Data were acquired by scan cycles of one
371 FTMS scan with a resolution of 60000 at m/z 400 and a range from 370 to 2000 m/z in parallel with six
372 MS/MS scans in the ion trap of the most abundant precursor ions. The mgf-files generated by Xcalibur
373 software (Thermo Scientific, Bremen, Germany) were used for database searches with the MASCOT
374 search engine (version 2.4.1, Matrix Science, London, UK) against the SwissProt database (Taxonomy
375 Mus musculus; version 2016_05). Peptide mass tolerance for database searches was set to 5 ppm and
376 fragment mass tolerance to 0.4 Da. Carbamidomethylation of C was set as fixed modification. Variable
377 modifications included oxidation of M, deamidation of NQ and phosphorylation STY. One missed
378 cleavage site in case of incomplete trypsin hydrolysis was allowed. Furthermore, proteins were
379 considered as identified if more than one unique peptide had an individual ion score exceeding the
380 MASCOT identity threshold (ion score cut-off of 22-23). Identification under the applied search
381 parameters refers to False Discovery Rate (FDR) < 3,5% and a match probability of $p<0.05$, where p is
382 the probability that the observed match is a random event.

383 <u>b. In mouse livers:</u> Protein digest and desalting as well as phosphopeptide enrichment were performed
384 as previously described [24]. Briefly, protein lysates were reduced with dithiothreitol (Merck) and
385 cysteine residues were alkylated with iodoacetamide (Merck). In-solution protein digestion was
386 performed using Lys-C (Wako Chemicals, Neuss) and trypsin (Promega). For analysis of the input
387 samples, a 10 µg aliquot of the digest was desalted with Pierce C18 spin columns (Thermo Fisher

388 Scientific) according to the manufacturer's instructions, with 1 µg subjected to analysis by LC-MS/MS.
389 The remaining part of the digest was acidified with TFA prior to desalting by solid-phase extraction
390 using Sep-Pak C18 cartridges (Sep-Pak tC18, 1 cc Vac (100 mg), Waters). Phosphopeptides were
391 enriched by titanium dioxide (TiO2) chromatography as described [24].

392 LC-MS/MS analysis was performed on a Q-Exactive HF mass spectrometer (Thermo Scientific) online
393 coupled to an Ultimate 3000 nano-RSLC (Dionex). Peptides were automatically loaded on a C18 trap
394 column (300 µm inner diameter (ID) × 5 mm, Acclaim PepMap100 C18, 5 µm, 100 Å, LC Packings) at
395 30µl/min flow rate prior to C18 reversed phase chromatography on the analytical column (nanoEase
396 MZ HSS T3 Column, 100Å, 1.8 µm, 75 µm x 250 mm, Waters) at 250nl/min flow rate in a 95 minutes
397 non-linear acetonitrile gradient from 3 to 40% in 0.1% formic acid. Profile precursor spectra from 300
398 to 1500 m/z were recorded at 60000 resolution with an automatic gain control (AGC) target of 3e6 and
399 a maximum injection time of 50 ms. TOP10 fragment spectra of charges 2 to 7 were recorded at 15000
400 resolution with an AGC target of 1e5, a maximum injection time of 150 ms for phospho-measurements
401 and 50 ms for measurements of unenriched samples, an isolation window of 1.6 m/z, a normalized
402 collision energy of 27 and a dynamic exclusion of 30 seconds.

403 Mass spectrometric raw data was processed separately for the phospho-enriched and non-enriched
404 fraction of samples with Progenesis QI for proteomics (Version 3.0, Nonlinear Dynamics, Waters) to
405 perform label-free quantification with pairwise normalization as described in [25, 26] and Proteome
406 Discoverer (Version 2.1.1.21, Thermo Fisher Scientific) using the Sequest HT search engine and the
407 ptmRS node for the confident localization of phosphosites [24].

408 **7. Cell or tissue lysis and co-immunoprecipitation (Co-IP)**

409 For co-IP experiments, cells and frozen liver tissues were lysed in ice-cold lysis CHAPS-buffer containing
410 10 mM KPO_4 (pH 7.2), 1 mM EDTA, 5 mM EGTA, 10 mM $MgCl_2$, 50 mM β-Glycerophosphate and
411 0.3% CHAPS supplemented with Complete Protease Inhibitor Cocktail (Roche, #11836145001) and
412 PhosSTOP EASYpack phosphatase inhibitor (Roche, #4906837001). Lysed cells or liver tissue were

413 centrifuged at 12.000 rpm for 5 minutes at 4°C and supernatants were collected. Protein
414 concentrations were measured with Bradford (BioRad, #5000006) or BCA assay (Pierce, #23227). For
415 immunoprecipitation of transfected cell lysates, anti-Flag affinity gel (Sigma, #A2220) or HA conjugated
416 agarose beads (Sigma, #A2095) were used. Prior to use, the beads were washed with lysis buffer via
417 centrifugation at 4.000 rpm for 2 minutes. For immunoprecipitation, cell lysates were incubated with
418 the beads for 2 hours at 4°C on a rotator. The beads were washed 3 times with ice-cold co-IP lysis
419 buffer with centrifugation steps in between. 2x laemmli buffer was added to the samples which then
420 were boiled at 95°C for 5 minutes.

421 Liver lysates of WT mice were prepared to analyze endogenous interaction of TSC22D4-Akt1. Rabbit
422 IgG control [1 mg/ml] (CST, #2729S) or TSC22D4 antibody (Pineda, home-made antibody, 1mg/ml)
423 were incubated with liver lysates at 4°C overnight on a rotating rack. Next day, protein A/G beads
424 (Santa Cruz, #sc-2003) were conjugated to protein-antibody complex with 2 hours of incubation at 4°C
425 on a rotating rack. The lysates were washed 3 times with lysis buffer and added 70 *µl of* 2x laemmli
426 sample buffer.

427 **8. Western blot analysis**

428 Protein extracts and immunoprecipitates were run on 10% (BioRad, #4561036) or any kD (BioRad,
429 #4569036) precast protein gels in sodium dodecyl sulfate (SDS) buffer followed by electrophoretic
430 transfer of proteins to nitrocellulose membrane (BioRad, #2895). After blocking in 5% nonfat dried milk
431 diluted in tris-buffered saline and 1% tween 20 (TBS-T) for 1 hour at RT, the membranes were
432 incubated with primary antibodies specific for TSC22D4 (home-made, by PINEDA Antibody Service,
433 Flag-HRP (#A8592, Sigma), HA (#2999, CST), Myc (#2040, CST), p-Akt (S473) (#4060, CST), p-Akt (T308)
434 (#13038, CST), Akt (#9272 ,CST), p-GSK3 beta (S9) (#05-643, Upstate), GSK3 beta (#05-412, Upstate),
435 p-Foxo1 (S256) (#9461, CST), Foxo1 (#2880, CST), p-p70S6K1 (#9234, CST), p70S6K1 (#9209, CST), pS6
436 (#2271, 2215), S6 (#2217, CST), pAMPK α T172 (#2531, CST), AMPK α (#2532, CST), VCP (ab11433,
437 Abcam). Primary antibodies were incubated in 3% BSA overnight at 4°C on a rocker. After 3 times wash

438 with TBS-T each for 10 minutes, membranes were incubated with HRP-conjugated secondary
439 antibodies targeting rabbit or mouse IgG for 1 hour at RT. To avoid background noise in endogenous
440 co-IP experiments, HRP-conjugated veriblot (Abcam, #131366) was used as secondary antibody.
441 Immunoblots were developed using ECL western blotting substrate (Sigma, #GERPN2209 or
442 Amersham, #GERPN2236). ChemiDoc Imaging System (BioRad) was used to detect and analyze
443 chemiluminescence signals.

444 **9. *In vitro* λ phosphatase assay**

445 Immunoprecipitated Flag-TSC22D4 was subjected to λ phosphatase assay as previously described [27].
446 Following Flag-TSC22D4 immunoprecipitation, beads were washed three times in IP lysis buffer
447 followed by two additional washes in ST buffer (50 mM Tris-HCl, pH 7.2; 150 mM NaCl). Beads were
448 then resuspended in 1x phosphatase buffer (50 mM Tris-HCl, pH 7.5, 100 mM NaCl, 2 mM dithiothreitol,
449 0.1 mM EGTA, 0.01% Brij 35) that contained 2 mM $MnCl_2$. Samples were incubated at 30°C for 30 min
450 in the absence or presence of λ -phosphatase (Invitrogen), and reactions were terminated by adding
451 EDTA, pH 8.0, to a 50 mM final concentration and sample buffer to a 1x final concentration.

452 **10. Software and Data analysis**

453 Adobe Illustrator and IBS (Illustrator for biological sequences) programs were used to create figures
454 and cartoons of deletion mutants.

455 **11. Image Editing**

456 For some figures, irrelevant lanes were removed from western blot images. Such modifications were
457 indicated with a thin black line on western blot figures.

458 **Acknowledgments**
459 We would like to thank Diane Fingar (University of Michigan, Ann Arbor, USA), Reuben Shaw (Salk
460 Institute for Biological Studies, San Diego, CA, USA), Thomas Fleming (Heidelberg University Hospital,

461 Germany) and Bilgehan Ibibik (Bilkent University, Ankara, Turkey) for their support during the
462 preparation of this manuscript.

463 **Bibliography**

464 1. Manning, B.D. and A. Toker, *AKT/PKB Signaling: Navigating the Network.* Cell, 2017. **169**(3):
465 p. 381-405.
466 2. Manning, B.D. and L.C. Cantley, *AKT/PKB signaling: navigating downstream.* Cell, 2007.
467 **129**(7): p. 1261-74.
468 3. Du, K. and P.N. Tsichlis, *Regulation of the Akt kinase by interacting proteins.* Oncogene, 2005.
469 **24**(50): p. 7401-9.
470 4. Jahn, T., et al., *Role for the adaptor protein Grb10 in the activation of Akt.* Mol Cell Biol, 2002.
471 **22**(4): p. 979-91.
472 5. Du, K., et al., *TRB3: a tribbles homolog that inhibits Akt/PKB activation by insulin in liver.*
473 Science, 2003. **300**(5625): p. 1574-7.
474 6. Demir, S., et al., *Emerging Targets in Type 2 Diabetes and Diabetic Complications.* Adv Sci
475 (Weinh), 2021. **8**(18): p. e2100275.
476 7. Ekim Ustunel, B., et al., *Control of diabetic hyperglycaemia and insulin resistance through*
477 *TSC22D4.* Nat Commun, 2016. **7**: p. 13267.
478 8. Kester, H.A., et al., *Transforming growth factor-beta-stimulated clone-22 is a member of a*
479 *family of leucine zipper proteins that can homo- and heterodimerize and has transcriptional*
480 *repressor activity.* J Biol Chem, 1999. **274**(39): p. 27439-47.
481 9. Canterini, S., et al., *Multiple TSC22D4 iso-/phospho-glycoforms display idiosyncratic*
482 *subcellular localizations and interacting protein partners.* FEBS J, 2013. **280**(5): p. 1320-9.
483 10. Canterini, S., et al., *Subcellular TSC22D4 localization in cerebellum granule neurons of the*
484 *mouse depends on development and differentiation.* Cerebellum, 2012. **11**(1): p. 28-40.
485 11. Dragotto, J., et al., *The interplay between TGF-beta-stimulated TSC22 domain family proteins*
486 *regulates cell-cycle dynamics in medulloblastoma cells.* J Cell Physiol, 2019. **234**(10): p.
487 18349-18360.
488 12. Canterini, S., et al., *THG-1pit moves to nucleus at the onset of cerebellar granule neurons*
489 *apoptosis.* Mol Cell Neurosci, 2009. **40**(2): p. 249-57.
490 13. Fiol, D.F., S.K. Mak, and D. Kultz, *Specific TSC22 domain transcripts are hypertonically induced*
491 *and alternatively spliced to protect mouse kidney cells during osmotic stress.* FEBS J, 2007.
492 **274**(1): p. 109-24.
493 14. Zhang, X., et al., *Promotion of cellular senescence by THG-1/TSC22D4 knockout through*
494 *activation of JUNB.* Biochem Biophys Res Commun, 2020. **522**(4): p. 897-902.

495 15. Jones, A., et al., *TSC22D4 is a molecular output of hepatic wasting metabolism.* EMBO Mol
496 Med, 2013. **5**(2): p. 294-308.
497 16. Yasukawa, T., et al., *NRBP1-Containing CRL2/CRL4A Regulates Amyloid beta Production by*
498 *Targeting BRI2 and BRI3 for Degradation.* Cell Rep, 2020. **30**(10): p. 3478-3491 e6.
499 17. McWilliam, H., et al., *Analysis Tool Web Services from the EMBL-EBI.* Nucleic Acids Res, 2013.
500 **41**(Web Server issue): p. W597-600.
501 18. Wright, P.E. and H.J. Dyson, *Intrinsically disordered proteins in cellular signalling and*
502 *regulation.* Nat Rev Mol Cell Biol, 2015. **16**(1): p. 18-29.
503 19. Cuevas-Velazquez, C.L., et al., *Intrinsically disordered protein biosensor tracks the physical-*
504 *chemical effects of osmotic stress on cells.* Nat Commun, 2021. **12**(1): p. 5438.
505 20. Wolff, G., et al., *Hepatocyte-specific activity of TSC22D4 triggers progressive NAFLD by*
506 *impairing mitochondrial function.* bioRxiv, 2021: p. 2021.12.17.473222.
507 21. Narvekar, P., et al., *Liver-specific loss of lipolysis-stimulated lipoprotein receptor triggers*
508 *systemic hyperlipidemia in mice.* Diabetes, 2009. **58**(5): p. 1040-9.
509 22. Zeigerer, A., et al., *Functional properties of hepatocytes in vitro are correlated with cell*
510 *polarity maintenance.* Exp Cell Res, 2017. **350**(1): p. 242-252.
511 23. Godoy, P., et al., *Recent advances in 2D and 3D in vitro systems using primary hepatocytes,*
512 *alternative hepatocyte sources and non-parenchymal liver cells and their use in investigating*
513 *mechanisms of hepatotoxicity, cell signaling and ADME.* Arch Toxicol, 2013. **87**(8): p. 1315-
514 530.
515 24. Rahm, M., et al., *Time-resolved phosphoproteomic analysis elucidates hepatic 11,12-*
516 *Epoxyeicosatrienoic acid signaling pathways.* Prostaglandins Other Lipid Mediat, 2020. **146**:
517 p. 106387.
518 25. Hauck, S.M., et al., *Deciphering membrane-associated molecular processes in target tissue of*
519 *autoimmune uveitis by label-free quantitative mass spectrometry.* Mol Cell Proteomics, 2010.
520 **9**(10): p. 2292-305.
521 26. Merl, J., et al., *Direct comparison of MS-based label-free and SILAC quantitative proteome*
522 *profiling strategies in primary retinal Muller cells.* Proteomics, 2012. **12**(12): p. 1902-11.
523 27. Acosta-Jaquez, H.A., et al., *Site-specific mTOR phosphorylation promotes mTORC1-mediated*
524 *signaling and cell growth.* Mol Cell Biol, 2009. **29**(15): p. 4308-24.

525

526

Figure 1: TSC22D4 interacts with Akt1

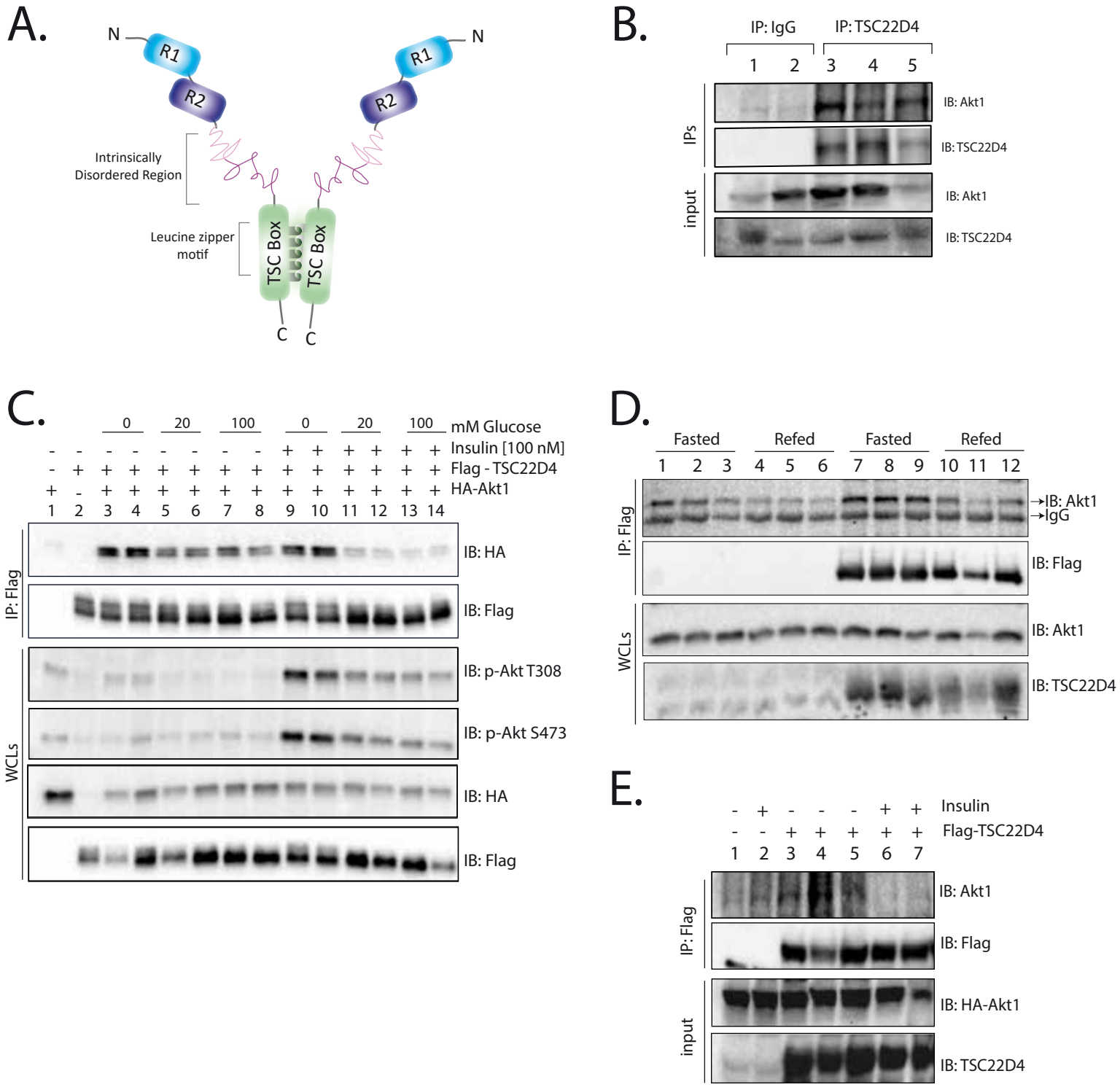

Figure 1. TSC22D4 interacts with Akt1. A. Illustration of TSC22D4 protein with evolutionarily conserved domains. **B.** Endogenous TSC22D4 from the wild type mouse liver lysates was immunoprecipitated (IP) with TSC22D4 antibody and the IPs and liver lysates (input) were immunoblotted (IB) with indicated antibodies. Normal rabbit IgG antibody was used as negative control to TSC22D4 antibody. **C.** Hepa 1-6 cells were transiently transfected with vector control or co-transfected with Flag-TSC22D4 (2,5 µg) and HA-Akt1 (2,5 µg) plasmids. 30 h posttransfection cells were serum and glucose starved overnight. Cells were pretreated without or with glucose [20 mM] for 30 min and incubated in the absence or presence of insulin [100 nM] for an additional 30 min and then lysed. Flag-TSC22D4 was immunopecipitated (IP) with anti-Flag affinity gel and the IPs and whole cell lysates (WCL) were immunblotted (IB) with indicated antibodies. **D.** Flag-TSC22D4 was IPed from the liver lysates of mice that were injected with adenoviruses containing empty vector control or Flag-TSC22D4 cDNA. The mice were starved for 16 h and refed the next day prior to sacrifice. The IPs and WCLs were IBed with indicated antibodies. **E.** Flag-TSC22D4 was immunoprecipitated (IP) with Flag affinity gel from liver lysates of 6 h starved and insulin injected mice (1.5U/kg for 10 min). IPs and whole liver lysates (input) were immunoblotted with indicated antibodies.

Figure 2. Stress signals promote TSC22D4-Akt1 interaction

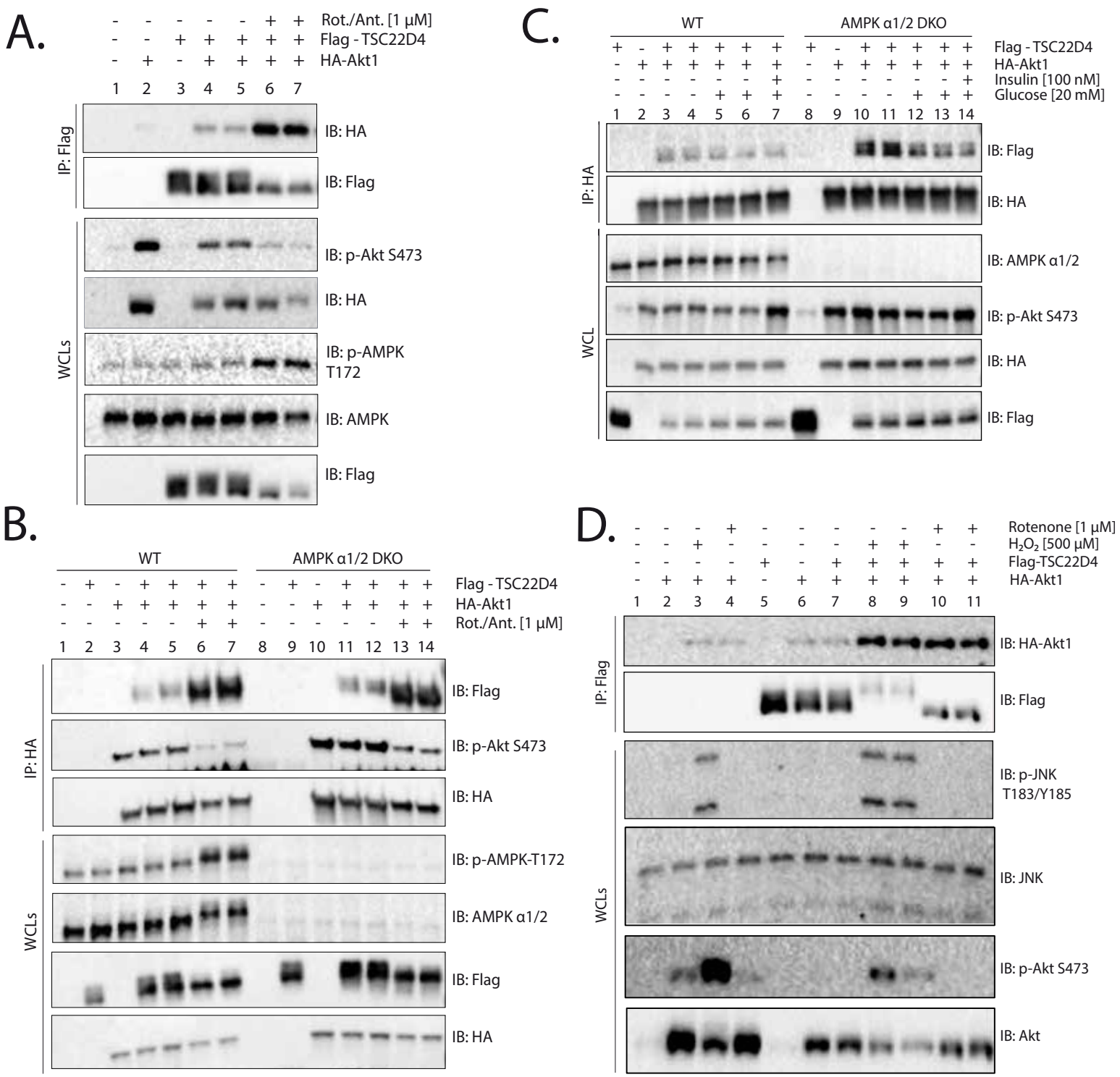

Figure 2. Stress signals promote TSC22D4-Akt1 interaction. A. Hepa 1-6 cells were transiently transfected with vector control or co-transfected with Flag-TSC22D4 (2,5 μg) and HA-Akt1 (2,5 μg) plasmids. 30 h posttransfection cells were serum and glucose starved overnight. Cells were pretreated without or with rotenone [1μM] and antimycin [1μM] mix 1 h prior to lysis. Flag-TSC22D4 was immunopecipitated (IP) with anti-Flag affinity gel and the IPs and whole cell lysates (WCL) were immunblotted (IB) with indicated antibodies. **B.** Similar to A except that WT or AMPKα1/2 Double Knockout U2OS cells were used and cells were starved for 4-6 h. IPs were performed with anti-HA antibody. **C.** WT and AMPKα1/2 Double Knockout U2OS cells were transiently transfected with vector control or co-transfected with Flag-TSC22D4 (2,5 μg) and HA-Akt1 (2,5 μg) plasmids. 48 h posttransfection cells were serum and glucose starved for 4-6 h. Cells were pretreated without or with glucose [10 mM] for 30 minutes and incubated in the absence or presence of insulin [100 nM] for an additional 30 min and then lysed. HA-Akt1 was immunopecipitated (IP) with anti-HA antibody and the IPs and whole cell lysates (WCL) were immunblotted (IB) with indicated antibodies. **D.** Hepa 1-6 cells were transiently transfected with vector control or Flag-TSC22D4 (2,5 μg) and HA-Akt1 (2,5 μg) plasmids. 30 h posttransfection cells were serum and glucose starved overnight. Cells were pretreated without or with H_2O_2 [500 μM] or Rotenone [1 μM] for an additional 1 h and then lysed. Flag-TSC22D4 was immunopecipitated (IP) with anti-Flag affinity gel and the IPs and WCLs were immunblotted (IB) with indicated antibodies.

Figure 3. D2 domain and TSC Box are required for TSC22D4-Akt1 interaction

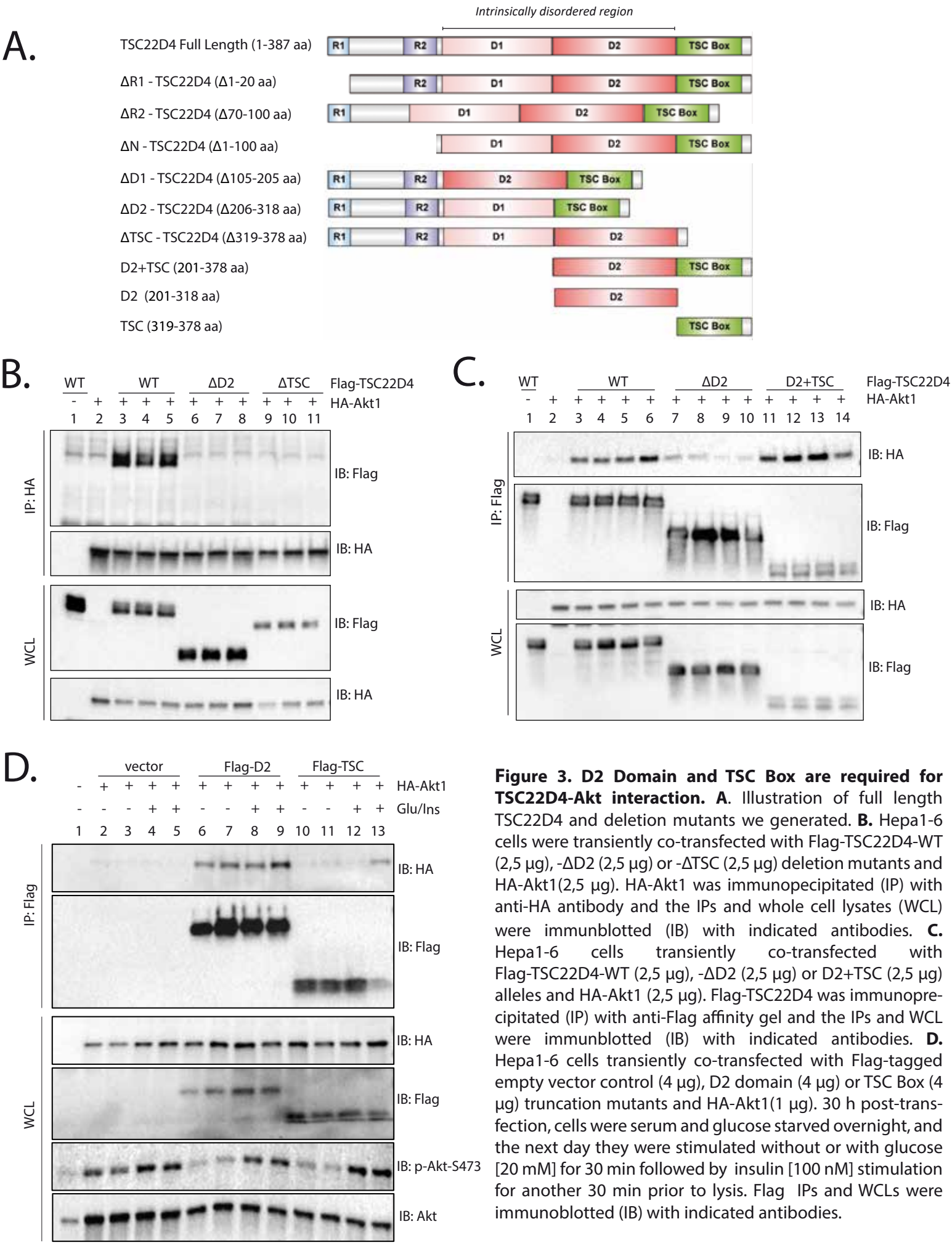

Figure 3. D2 Domain and TSC Box are required for TSC22D4-Akt interaction. A. Illustration of full length TSC22D4 and deletion mutants we generated. **B.** Hepa1-6 cells were transiently co-transfected with Flag-TSC22D4-WT (2,5 µg), -ΔD2 (2,5 µg) or -ΔTSC (2,5 µg) deletion mutants and HA-Akt1(2,5 µg). HA-Akt1 was immunopecipitated (IP) with anti-HA antibody and the IPs and whole cell lysates (WCL) were immunblotted (IB) with indicated antibodies. **C.** Hepa1-6 cells transiently co-transfected with Flag-TSC22D4-WT (2,5 µg), -ΔD2 (2,5 µg) or D2+TSC (2,5 µg) alleles and HA-Akt1 (2,5 µg). Flag-TSC22D4 was immunoprecipitated (IP) with anti-Flag affinity gel and the IPs and WCL were immunblotted (IB) with indicated antibodies. **D.** Hepa1-6 cells transiently co-transfected with Flag-tagged empty vector control (4 µg), D2 domain (4 µg) or TSC Box (4 µg) truncation mutants and HA-Akt1(1 µg). 30 h post-transfection, cells were serum and glucose starved overnight, and the next day they were stimulated without or with glucose [20 mM] for 30 min followed by insulin [100 nM] stimulation for another 30 min prior to lysis. Flag IPs and WCLs were immunoblotted (IB) with indicated antibodies.

Figure 4. TSC22D4 undergoes phosphorylation

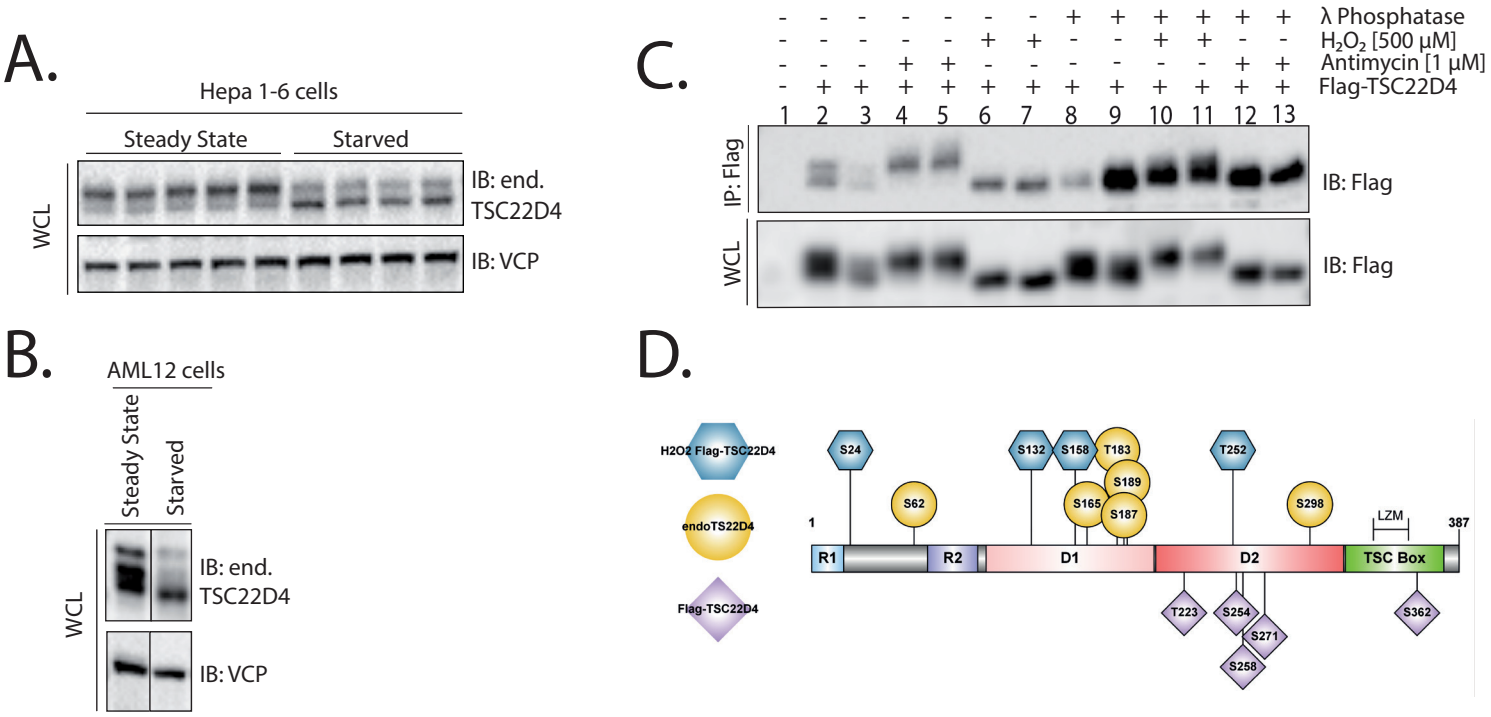

Figure 4. TSC22D2 undergoes phosphorylation. A and B. Hepa 1-6 cells (A) and AML12 (B) cells were grown under steady state conditions and were starved or not starved in the absence of glucose and serum for 16 h. Cells were lysed the next day and the whole cell lysates (WCL) were immunoblotted (IB) with indicated antibodies. **C.** Hepa 1-6 cells were transiently transfected with Flag-TSC22D4. 24 h posstransfection cells were treated with H_2O_2 or antimycin for 1 h prior to lysis. Flag-TSC22D4 was immunoprecipitated (IP) with anti-Flag affinity gel. IPed Flag-TSC22D4 was subjected to in vitro λ phosphatase treatment. The IPs and WCL were immunoblotted with indicated antibodies. **D.** TSC22D4 phosphorylation sites (p-sites) identified by LC-MS/MS. Yellow: p-sites that are identified on endogenous TSC22D4 in Hepa 1-6 cells (S165) or in mouse livers (S62, T183, S187, S189, S298). P-sites that are identified on transiently transfected Flag-TSC22D4 without or with H_2O_2 treatment are indicated in purple and blue, respectively. LZM: Leucine Zipper Motif

Supplementary Figure 1

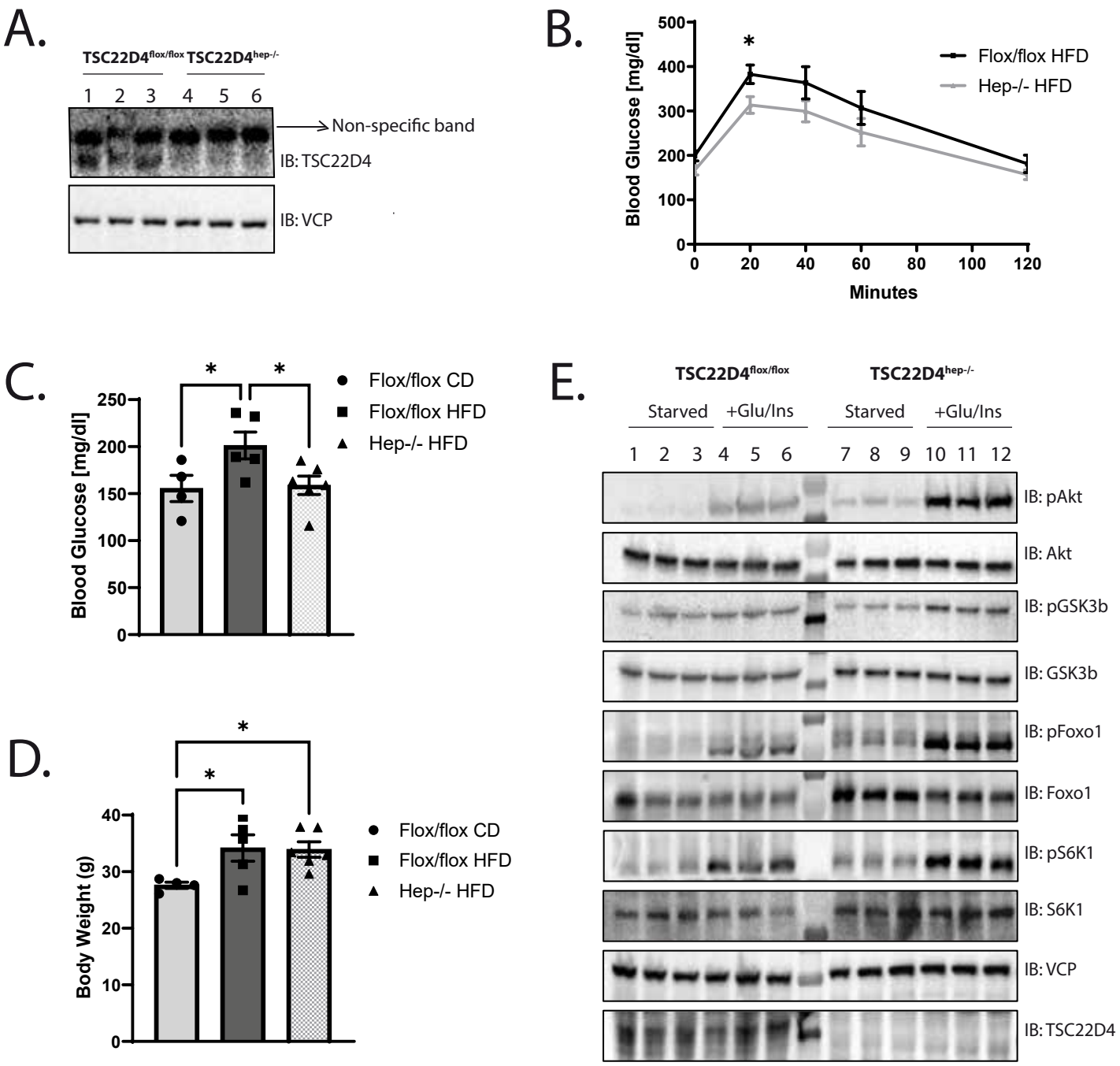

Supplementary Figure 1. **Hepatocyte specific TSC22D4 knockout (TSC22D4$^{hep-/-}$) mice show imroved glucose handling. A.** Western blot analysis of the mouse liver lysates from TSC22D4$^{flox/flox}$ control mice or TSC22D4$^{hep-/-}$ mice immunoblotted with indicated antibodies. **B.** Intraperitoneal glucose tolerance test (i.p. GTT) performed with mice as in A subjected to high fat diet (HFD) for 6 weeks. Mice were fasted for 6 h of followed by glucose solution injection at a dose of 1g/kg mouse weight. n=5-6 per group. Statistical analysis: 2-way ANOVA with repeated measures and Fisher's LSD test. **C.** Fasting blood glucose levels of TSC22D4$^{flox/flox}$ and TSC22D4$^{hep-/-}$ mice on 9 weeks of control diet (CD) or HFD challenge . Statistical analysis 2-way ANOVA and Fisher's LSD test. **D.** Body weight of mice as in C. Statistical analysis 2-way ANOVA and Dunnet's multiple comparisons test. **E.** Western blot analysis of primary hepatocytes of TSC22D4$^{flox/flox}$ control mice and TSC22D4$^{hep-/-}$ mice in starved or glucose and insulin stimulated conditions immunoblotted (IB) with indicated antibodies.

Supplementary Figure 2

CLUSTAL O (1.2.3) multiple sequence alignment –

```
gi|733215333|ref|NP_001289972.1|Human   MSGGKKKSSFQITSVTTDYEGPGSPGASDPPTPQPPT-------GPPPRLPNGEPSPDPG    53
gi|311251027|ref|XP_003124405.1|Pig     MSGGRKKSSFQITSVTTDYEGPGSPGGSDPPALPAPT-------GPPPRLPNGEPNPEPG    53
gi|75750501|ref|NP_076399.4|    Mouse   MSGGKKKSSFQITSVTTDYEGPGSPGASDSPVPPALA-------GPPPRLPNGDPNPDPG    53
gi|1072286148|ref|XP_018429460.1Frog    MSLGKKRSGFQITSVTSDYLPSSPLSPVSPNHSE----------------PSSSPTPPNG    44
gi|884983148|ref|XP_012987990.1|Fish    MSGGKKRSGFKITSVTSGEAPPPASSSSQSSHSPQSSSQAAASSKPGSSHQQGSSSQPTT    60
                                        ** *:*:*.*:*****:.       .  .                     ... .

gi|733215333|ref|NP_001289972.1|Human   GKGTPRNGSPPPGAPSSRFRVVKLP---HGLGEPYRRGRWTCVDVYERDLEPHSFGGLLE    110
gi|311251027|ref|XP_003124405.1|Pig     GRGTPRNGSPPPGAPASRFRVVKLP---QGLGEPYRRGRWTCVDVYERDLEPPSFGRLLE    110
gi|75750501|ref|NP_076399.4|    Mouse   GRGTPRNGSPPPGAPASRFRVVKLP---QGLGEPYRRGRWTCVDVYERDLEPPSFGRLLE    110
gi|1072286148|reXP_018429460.1| Frog   ----------PRSPPASRFRLVRLDQDPLGGGRRYQKGRWTCVDFYHLDVGAQQRAGAG-    93
gi|884983148|ref|XP_012987990.1|Fish    PRSLRKYNSHDSTGQGSRFRVVRLG---QGHGEPYRRGRWICTDFLEREEG-VGFRRVMD    116
                                                  .****:*:*     * *. *::*** *.*. . :

gi|733215333|ref|NP_001289972.1|Human   GIRG--------------ASGGAGGRSLDSRLELASLGLGAPTPPSGLSQGPTSWLRPPP    156
gi|311251027|ref|XP_003124405.1|Pig     GIRG--------------ASGGTGGRSLDSRLELASLGLSAPAPQPGLSQGPTSWLRPPP    156
gi|75750501|ref|NP_076399.4|    Mouse   GIRG--------------ASGGTGGRSLDSRLELASLGISTPIPQPGLSQGPTSWLRPPP    156
gi|1072286148|refXP_018429460.1|Frog    -------------------------HSLDSGLPRAAP----AIPPLLLSPGAGAKGQQAP    124
gi|884983148|ref|XP_012987990.1|Fish    SMRHAHSLESLEGIGLERVGGGAGGGLLGHMPALRAGN-------LVHSQGTTHLLAQPI    169
                                                                  *.      :           * *

gi|733215333|ref|NP_001289972.1|Human   TSPGPQARSFTGGLGQLVV----PSKA---KAEKP--------------------PLSASS    190
gi|311251027|ref|XP_003124405.1|Pig     TSPGPQARSLTGGLGQLAV----PSKA---KVETP--------------------PLSVSP    190
gi|75750501|ref|NP_076399.4|    Mouse   TSPGPQARSFTGGLGQLAG----PGKA---KVETP--------------------PLSASP    190
gi|1072286148|refXP_018429460.1|Frog    RSQGAP--ILT-GVTDRETTAQPASRLRLVRLDQDPLGGGRRYQKGRWTCVDFYHLDVGA    181
gi|884983148|ref|XP_012987990.1|Fish    GSEGEGF----GGFKPLFLHSGPPSPT---NLDRS--------------------NLRVVD    203
                                         * *        *.          .     . :                      * .

gi|733215333|ref|NP_001289972.1|Human   PQQRPPEPETGESAGTSRAATPLPSLRVEAEAGGSGARTPPLSRRKAVDMRLRMELGAPE    250
gi|311251027|ref|XP_003124405.1|Pig     PQQRPPEPGTGDSTGTSRAATPLPSLRVEVEAGGSTAGTPPLPWTKDGALRLRME-----    245
gi|75750501|ref|NP_076399.4|    Mouse   PQQRPPGPGTGDSA------QTLPSLRVEVESGGSAAATPPLSRRRDGAVRLRMELVAPA    244
gi|1072286148|re|XP_018429460.1|Frog   -QQ-RAGAGHSLDSGLPRAAPAIPPLLLSPGAGAKGQQAPRSQ---GAP--ILTGVTDRE    234
gi|884983148|ref|XP_012987990.1|Fish    SMPPPPSPR---------PRNIPPPLRLDVDASGRSL--------------LRV----SH    236
                                                             * * :.  :..                :

gi|733215333|ref|NP_001289972.1|Human   EMGQVPPLDSRPSSPALYFTHDASLVHKSPDPFGAVAAQKFSLAHSMLAISG--HLDSDD    308
gi|311251027|ref|XP_003124405.1|Pig     ETGQVPPLDSRPGSPALYFFPEASLVRKSPDPFGAAAAQSLSLARSMLAISG--HLDSDD    303
gi|75750501|ref|NP_076399.4|    Mouse   ETGKVPPTDSRPNSPALYF--DASLVHKSPDPFGAAAAQSLSLARSMLAISG--HLDSDD    300
gi|1072286148|refXP_018429460.1|Frog    TTAQLSPLP-QPASPIITVQSDNR----PSRPKSDVFNERLLLAQTVFRMGD----GNDQ    285
gi|884983148|ref|XP_012987990.1|Fish    SQPSSPPLQGKDGT----FLPSLT-------PI------QTPSAWSMFGTGGDFHLLGED    279
                                           .  *   :  :    .  .         *           * :::  ..     .::

gi|733215333|ref|NP_001289972.1|Human   DSGSGSLVGIDNKIEQAMDLVKSHLMFAVREEVEVLKEQIRELAERNAALEQENGLLRAL    368
gi|311251027|ref|XP_003124405.1|Pig     DSGSGSLVGIDNKIEQAMDLVKSHLMFAVREEVEVLKEQIRDLAERNAALEQENGLLRAL    363
gi|75750501|ref|NP_076399.4|    Mouse   DSGSGSLVGIDNKIEQAMDLVKSHLMFAVREEVEVLKEQIRDLAERNAALEQENGLLRAL    360
gi|1072286148|refXP_018429460.1|Frog    DSAPNSTGAIDNKIEQAMDLVKTHLLFAVREEVEALKEQIKELADRNALLEHENNLLRTL    345
gi|884983148|ref|XP_012987990.1|Fish    SGSNSSMIAIDNKIEQAMDLVKTHLMLAVREEVELLREQIKELSDRNVQLERENYILRTL    339
                                        ... .*  .*************:**::******* *:***::*::**. **:** :**:*

gi|733215333|ref|NP_001289972.1|Human   ASPEQLAQLPSSGVPRLGPPAPNGPSV--------------------------------    395
gi|311251027|ref|XP_003124405.1|Pig     ASPEQLAQLPSSGVPRLGPPAPNGPSV--------------------------------    390
gi|75750501|ref|NP_076399.4|    Mouse   ASPEQLAQLPSSGLPRLGPSAPNGPSI--------------------------------    387
gi|1072286148|ref|XP_018429460.1Frog   ASPQQLSELVARIKA-SGKGDVLGTKIYSYRYSSAWRNLILQDDHENGPLRNLSARRPST    404
gi|884983148|ref|XP_012987990.1|Fish    GHRD-------------------------------------------------------    343
                                        .  :
```

Supplementary Figure 2. CLUSTAL Omega multiple sequence alignment analysis of TSC22D4
Highlighted in blue: Evolutionarily conserved regions on TSC22D4 primary amino acid sequence.
Highlighted in pink: Leucine Zipper Motif
Highlighted in yellow: Novel phosphorylation sites on TSC22D4 identified via LC/MS-MS

Supplementary Figure 3

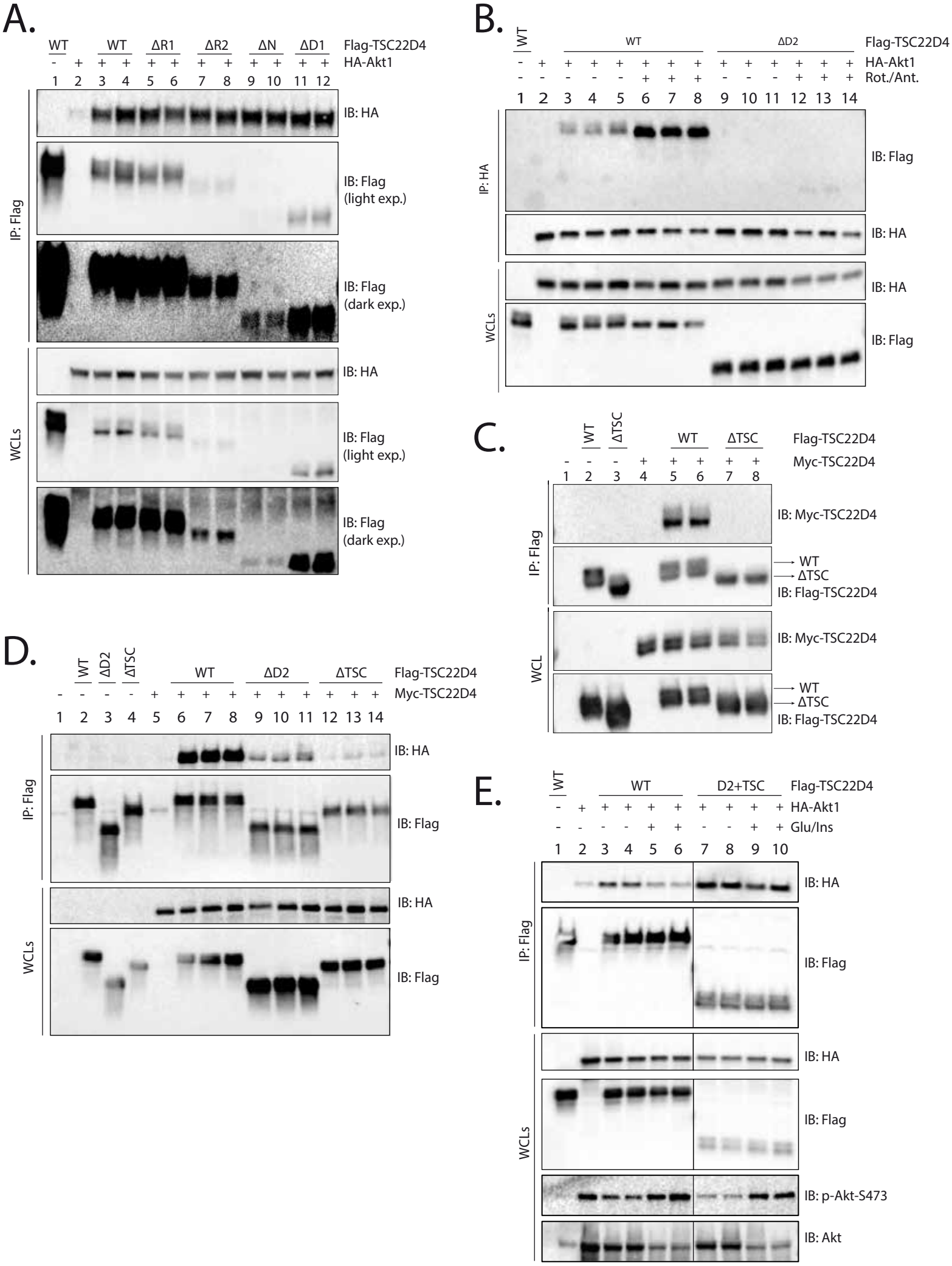

Supplementary Figure 3. Mapping the Akt1 interaction domains on TSC22D4 . A. Hepa1-6 cells were transiently co-transfected with Flag-TSC22D4-WT (2,5 µg), -ΔR1 (2,5 µg), -ΔR2 (2,5 µg), -ΔN (2,5 µg) or -ΔD1 (2,5 µg) deletion mutants and HA-Akt1(2,5 µg). Flag-TSC22D4 was immunopecipitated (IP) with anti-Flag affinity gel and the IPs and WCLs were immunblotted (IB) with indicated antibodies. **B.** Hepa1-6 cells were transiently co-transfected with Flag-TSC22D4-WT (2,5 µg) or -Δ D2 (2,5 µg) and HA-Akt1 (2,5 µg). 30 h post transfection, cells were serum and glucose starved overnight and the next day, they were treated without or with Rotenone/Antimycin [1 µg] for 1 h prior to cell lysis. IPs were performed with anti-HA antibody. IPs and WCLs were immunblotted (IB) with indicated antibodies. **C.** Hepa1-6 cells were transiently co-transfected with Flag-TSC22D4-WT (2,5 µg) or -ΔTSC (2,5 µg) and Myc-TSC22D4-WT (2,5 µg). Flag-TSC22D4 alleles were immunoprecipitated with anti-Flag affinity gel (IP) and WCLs were immunoblotted (IB) with indicated antibodies. **D.** Hepa1-6 cells were transiently co-transfected with Flag-TSC22D4-WT (2,5 µg), -ΔD2 (2,5 µg) or -ΔTSC (2,5 µg) and Myc-TSC22D4-WT (2,5µg). Flag IPs and WCLs were immunoblotted (IB) with indicated antibodies. **E.** Hepa1-6 cells were transiently co-transfected with Flag-tagged WT-TSC22D4 (2,5 µg) or D2+TSC (2,5 µg) and HA-Akt1 (2,5 µg). 30 h post transfection, cells were serum and glucose starved overnight and the next day, they were stimulated without or with glucose [20 mM] for 30 minutes and insulin [100 nM] for another 3o minutes. Flag IPs and WCLs were immunblotted (IB) with indicated antibodies.